Kadari Johanaus Kepler. et.al, International Journal of Engineering Research and Applications
www.ijera.com
ISSN: 2248-9622, Vol. 15, Issue 5, May 2025, pp 47-54

RESEARCH ARTICLE OPEN ACCESS

Structural and Modal Analysis of Drive Axle with Material Optimization for Heavy Loads

Kadari Johanaus Kepler*, Kaaligi Banashanker*, Chitty Kushal Kumar*,
Dr. Gadipelly Bhaskar** Dr. M. Udaya Kumar***
**(Student, Department of Mechanical Engineering, Methodist College of Engineering and Technology, Hyderabad-01)*
***(Assistant professor, Department of Mechanical Engineering, Methodist College of Engineering and Technology, Hyderabad-01)*
****(Associate professor, Department of Mechanical Engineering, Methodist College of Engineering and Technology, Hyderabad-01)*

ABSTRACT
Drive axles in heavy-load vehicles play a crucial role in power transmission and load-bearing under demanding conditions. This study presents a comprehensive structural and modal analysis of a drive axle using Finite Element Analysis (FEA) to evaluate its performance under real-world operating loads. A detailed 3D CAD model was developed and analyzed in ANSYS Workbench to assess stress distribution, deformation patterns, and fatigue life. Modal analysis was conducted to determine natural frequencies and vibration characteristics, crucial for preventing resonance-induced failures.

The research compares multiple materials to identify optimal combinations of strength, weight reduction, and fatigue resistance. Results demonstrate that advanced materials can significantly improve axle performance while reducing overall weight. The optimized design enhances load distribution, increases durability, and lowers manufacturing costs. These findings have broad applications across conventional, electric, and hybrid heavy vehicles, contributing to more efficient and sustainable automotive designs.

This work aligns with modern engineering priorities of lightweight construction and material efficiency, offering valuable insights for the development of next-generation drive train components. The methodology and results provide a practical framework for improving axle design while maintaining structural integrity under extreme operating conditions.

Keywords - Drive axle, Finite element analysis, Heavy vehicles, Material selection and Structural optimization.

Date of Submission: 01-05-2025 Date of acceptance: 09-05-2025

I. INTRODUCTION

In the dynamic realm of mechanical and automotive engineering, drive train systems serve as the critical link between power generation and vehicle movement. The drive axle, particularly in heavy-load vehicles such as commercial trucks, buses, and construction machinery, plays a dual role—transmitting torque from the differential to the wheels while simultaneously supporting substantial structural loads. Beyond its primary function, the axle must endure complex stresses, including bending, torsion, and impact forces, making its reliability essential for vehicle safety, fuel efficiency, and operational performance.

1.1 Background

Traditional drive axles have predominantly relied on forged steel and cast iron, materials selected for their high strength and durability. However, these conventional choices come with inherent limitations, most notably their excessive weight, which increases un-sprung mass, elevates fuel consumption, and places additional strain on suspension and braking systems. Furthermore, dynamic operating conditions—such as uneven terrain, variable loads, and high-speed vibrations—can induce fatigue, leading to premature axle failure.

The automotive industry's growing emphasis on sustainability and light weighting has prompted a re-evaluation of drive axle design. Modern engineering solutions now prioritize weight reduction without sacrificing structural integrity. Achieving this balance requires advanced analytical techniques, including **structural analysis** to assess stress distribution, deformation, and fatigue life, and **modal analysis** to identify natural frequencies and mitigate resonance risks. By leveraging these methods, engineers can optimize material selection and design, ensuring enhanced durability, efficiency, and performance in next-generation drive trains.

II. METHODOLOGY

Presents a systematic research framework for conducting structural and modal analysis of a heavy-load vehicle drive axle, with the ultimate objective of material optimization. The methodology integrates advanced computational techniques with empirical validation to ensure robust and practical outcomes.

STRESS ANALYSIS:

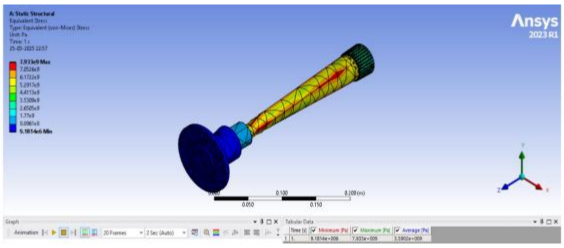

Fig.2.0 Stress Analysis of Shaft – Material: AISI 4140

A static structural analysis was conducted in ANSYS 2023 R1 to evaluate the equivalent (von Mises) stress distribution in an AISI 4140 steel shaft under a torsional load of 8829 N·m. The shaft was fixed at the flange side, with torque applied at the opposite end. Maximum stress reached 7.933 GPa, with stress concentrations observed near the shaft-flange transition due to geometric discontinuity.

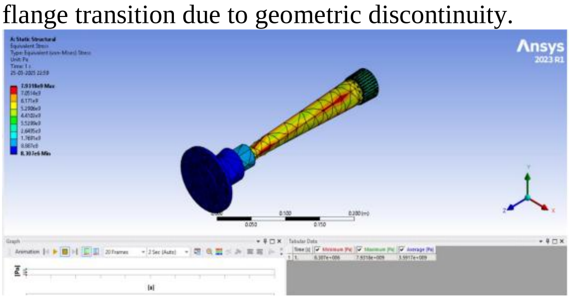

Fig.2.1 Stress Analysis of Shaft – Material: Aluminium Alloy

A static structural analysis was performed to study the equivalent (von Mises) stress distribution in an Aluminium Alloy 6061-T6 shaft under torsional loading. Stress visualization through a contour plot (red: high stress, blue: low stress) revealed a significant concentration near the diameter transition close to the fixed support, with a maximum stress of 7.931 GPa and minimum of 8.307 MPa**.**

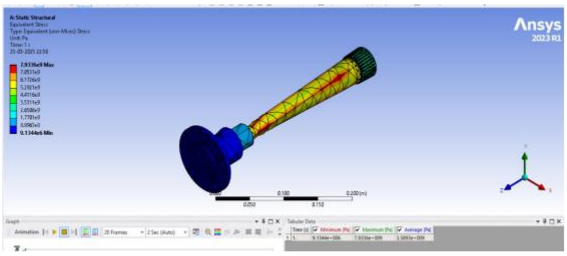

Fig.2.2 Stress Analysis of Shaft – Material: Ductile Cast Iron

The Equivalent Stress distribution in the Ductile Cast Iron shaft, shown via a color contour plot (red: maximum, blue: minimum), highlights a peak stress of 7.933 GPa at the diameter transition near the fixed support. Stress gradually decreases toward the free end, with the minimum stress of 9.134 MPa occurring at the flanged end.

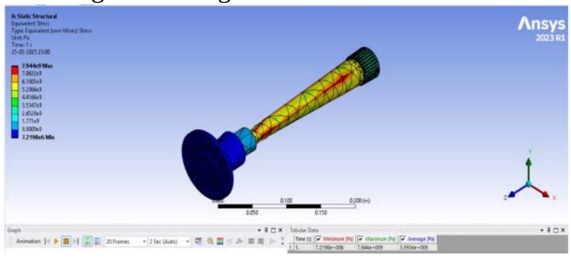

Fig.5.3 Stress Analysis of Shaft – Material: Ti-6Al-4V (Titanium Alloy)

The maximum stress of 7.944 GPa occurs at the transition between the shaft's smaller and larger diameter sections near the fixed support, while the minimum stress of 7.219 MPa appears at the flanged end. Stress distribution is non-uniform, with a critical concentration at the transition region, posing a significant structural concern**.**

DEFORMATION ANALYSIS:

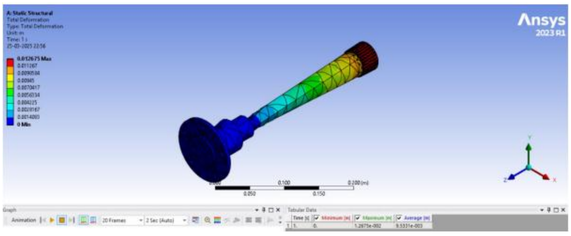

Fig.2.4 Deformation Analysis of Shaft – Material: AISI 4140

Static structural analysis in ANSYS 2023 R1 showed that under an applied moment of 8829 N·m, the shaft experienced a maximum deformation of 12.675 mm at the free end and zero deformation at the fixed support. Deformation increased gradually along the shaft in a twisting pattern, consistent with torsional loading behavior and boundary conditions.

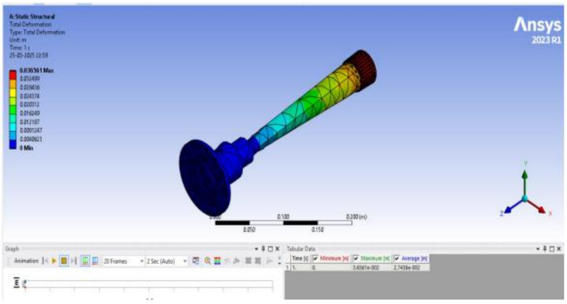

Fig.2.5 Deformation Analysis of Shaft – Material: Aluminium Alloy 6061-T6

The total deformation of the Aluminium Alloy 6061-T6 shaft under torsional loading is visualized using a color contour plot, with a maximum deformation of 36.561 mm at the free end. Deformation increases linearly from the fixed support to the free end, consistent with torsional behavior, indicating substantial twisting along the shaft.

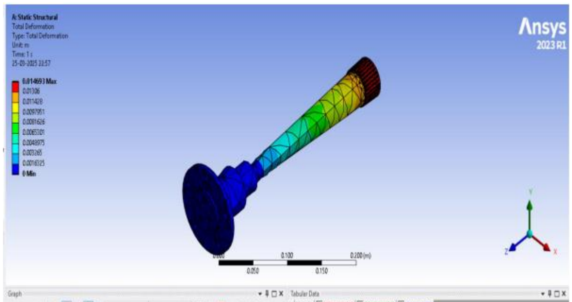

Fig.2.6 Deformation Analysis of Shaft – Material: Ductile Cast Iron

The total deformation of the Ductile Cast Iron shaft, visualized through a color contour plot, shows a maximum deformation of 14.693 mm at the free end, consistent with the location of the applied moment. Deformation increases linearly from the fixed support to the free end, with the minimum deformation occurring at the fixed support due to the boundary condition.

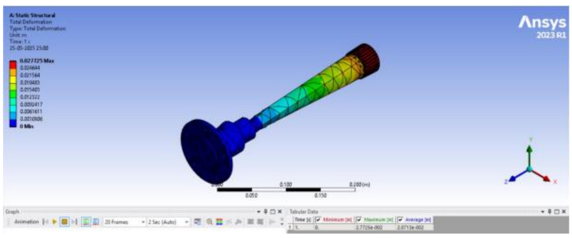

Fig.2.7 Deformation Analysis of Shaft – Material: Ti-6Al-4V Titanium Alloy

The total deformation of the Ti-6Al-4V Titanium Alloy shaft, shown through a color contour plot, reaches a maximum of 27.725 mm at the free end, consistent with the applied moment. Deformation increases linearly from the fixed support to the free end, and the observed deformation is between that of Aluminium Alloy 6061-T6 (36.561 mm) and Ductile Cast Iron (14.693 mm), indicating Ti-6Al-4V's intermediate stiffness.

MODAL ANALYSIS:

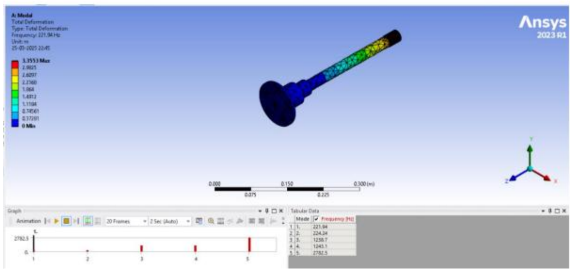

Fig.2.8 Modal Analysis - Mode 1 (Aluminium Shaft)

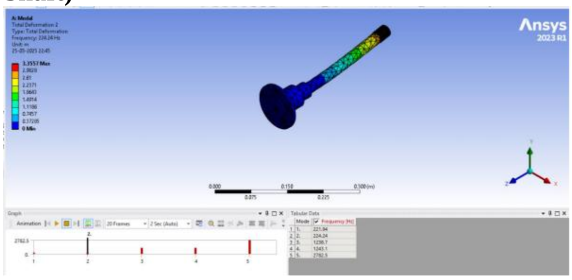

Fig.2.9 Modal Analysis - Mode 2 (Aluminium Shaft)

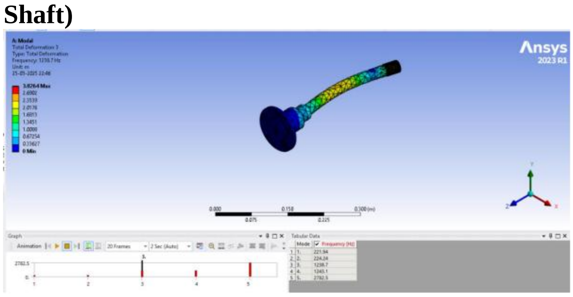

Fig.2.10 Modal Analysis - Mode 3 (Aluminium Shaft)

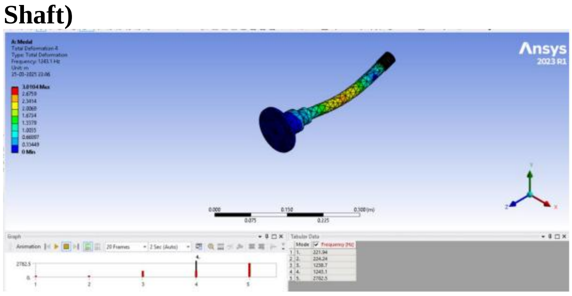

Fig.2.11 Modal Analysis - Mode 4 (Aluminium Shaft)

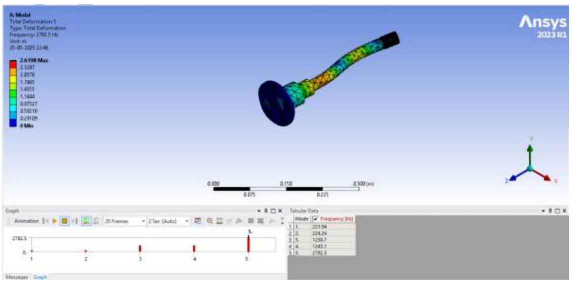

Fig.2.12 Modal Analysis - Mode 5 (Aluminium Shaft)

The modal analysis of the Aluminium shaft reveals the deformation patterns for Modes 1 through 5. Mode 1 (221.94 Hz) and Mode 2 (224.24 Hz) exhibit bending with maximum displacement at the free end, while Modes 3 (1238.7 Hz) and 4 (1243.1 Hz) show more complex bending and twisting. Mode 5 (2782.5 Hz) displays the most intricate bending and twisting deformation along the shaft.

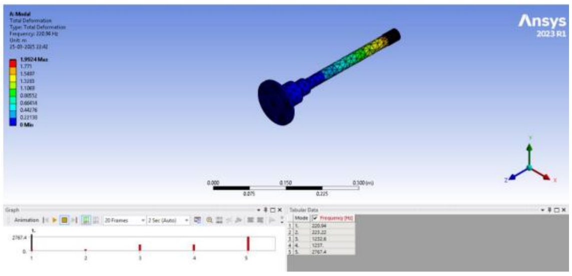

Fig.2.13 Modal Analysis - Mode 1 (AISI 4140 Shaft)

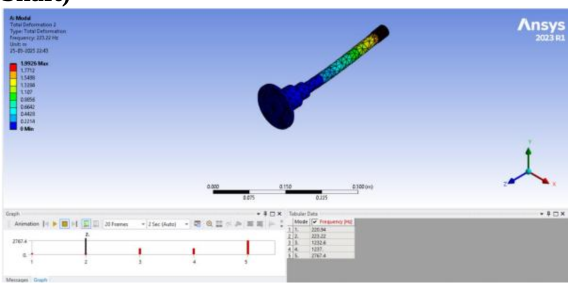

Fig.2.14 Modal Analysis - Mode 2 (AISI 4140 Shaft)

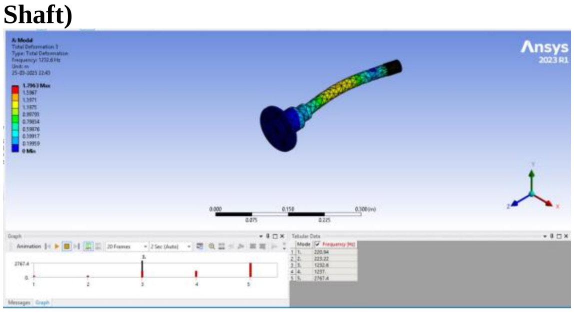

Fig.2.15 Modal Analysis - Mode 3 (AISI 4140 Shaft)

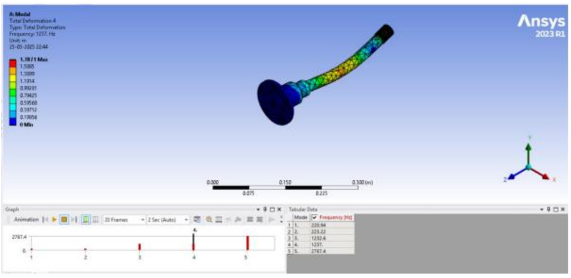

Fig.2.16 Modal Analysis - Mode 4 (AISI 4140 Shaft)

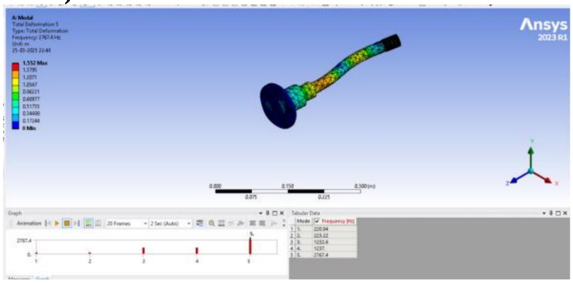

Fig.2.17 Modal Analysis - Mode 5 (AISI 4140 Shaft)

The modal analysis of the AISI 4140 shaft shows deformation patterns for Modes 1 to 5, with Mode 1 (220.94 Hz) and Mode 2 (223.22 Hz) exhibiting bending with maximum displacement at the free end. Modes 3 (1232.6 Hz) and 4 (1237 Hz) show more complex bending and twisting, while Mode 5 (2767.4 Hz) displays the most intricate deformation along the shaft.

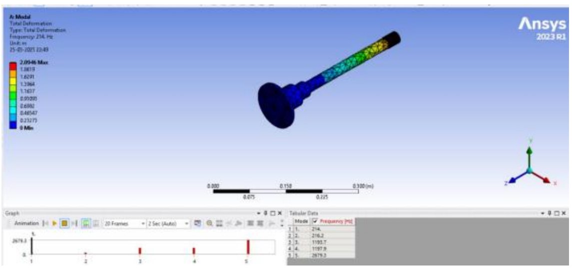

Fig.2.18 Modal Analysis - Mode 1 (Ductile Cast Iron Shaft)

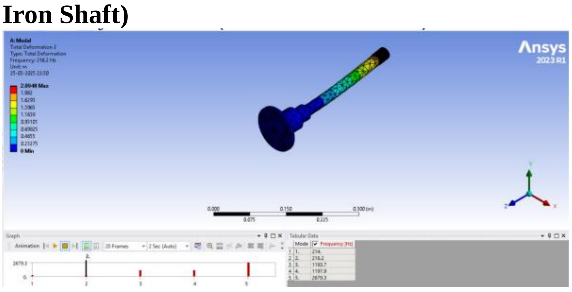

Fig.2.19 Modal Analysis - Mode 2 (Ductile Cast Iron Shaft)

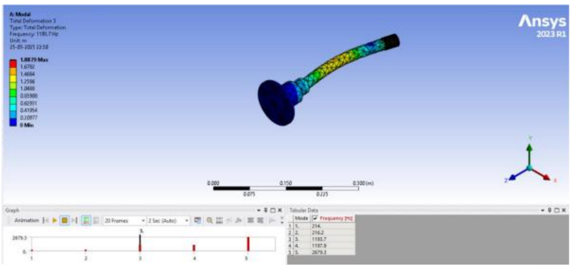

Fig.2.20 Modal Analysis - Mode 3 (Ductile Cast Iron Shaft)

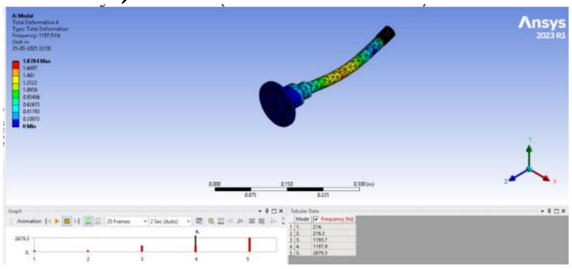

Fig.2.21 Modal Analysis - Mode 4 (Ductile Cast Iron Shaft)

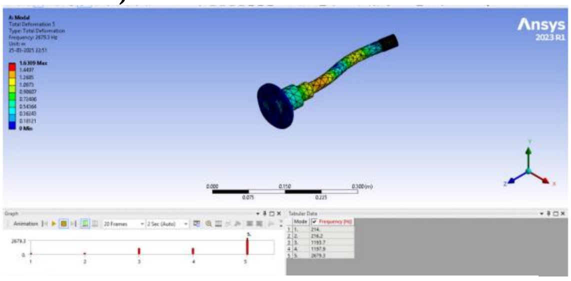

Fig.2.22 Modal Analysis - Mode 5 (Ductile Cast Iron Shaft)

The modal analysis of the Ductile Cast Iron shaft reveals deformation patterns for Modes 1 to 5, with Mode 1 (214 Hz) and Mode 2 (216.2 Hz) exhibiting bending modes with significant displacement at the free end. Modes 3 (1193.7 Hz) and 4 (1197.9 Hz) show more complex bending and twisting, while Mode 5 (2679.3 Hz) displays intricate deformation, indicating a higher level of complexity in the shaft's response to dynamic excitation.

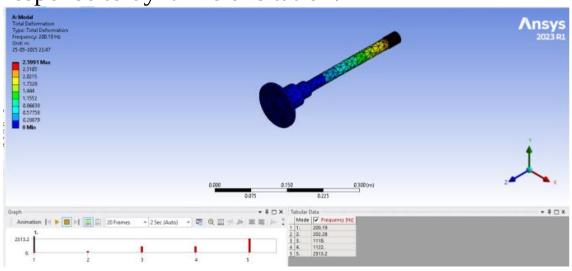

Fig.2.23 Modal Analysis - Mode 1 (Ti-6Al-4V) Titanium Alloy Shaft

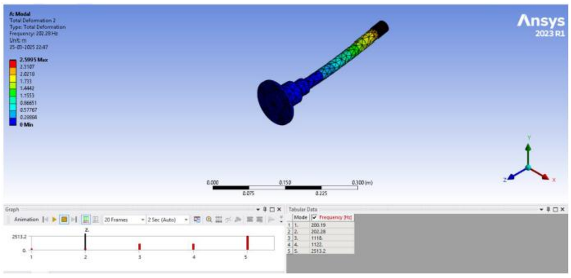

Fig.2.24 Modal Analysis - Mode 2 (Ti-6Al-4V) Titanium Alloy Shaft

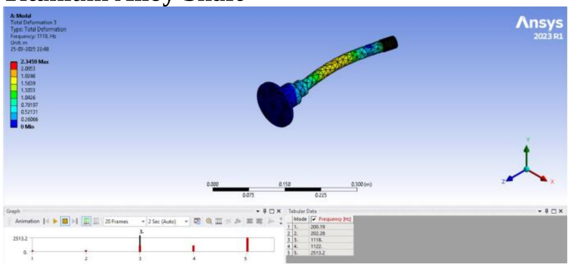

Fig.2.25 Modal Analysis - Mode 3 (Ti-6Al-4V) Titanium Alloy Shaft

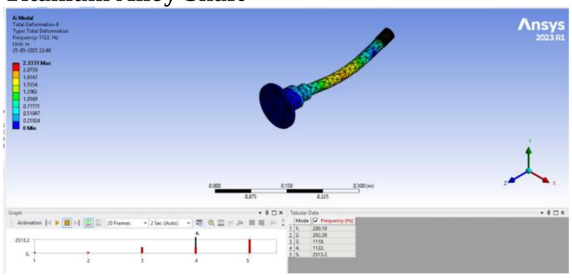

Fig.2.26 Modal Analysis - Mode 4 (Ti-6Al-4V) Titanium Alloy Shaft

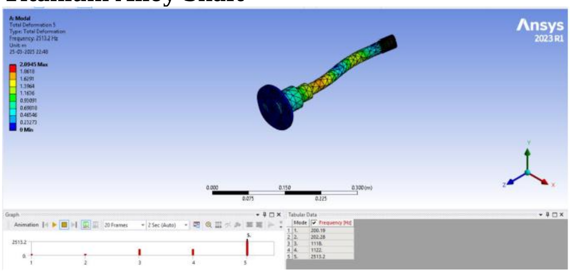

Fig.2.27 Modal Analysis - Mode 5 (Ti-6Al-4V) Titanium Alloy Shaft

The modal analysis of the Ti-6Al-4V Titanium Alloy shaft reveals deformation patterns for Modes 1 to 5, with Mode 1 (102.19 Hz) and Mode 2 (202.28 Hz) exhibiting bending modes with significant displacement at the free end. Modes 3 (1118 Hz) and 4 (1122 Hz) show more complex bending and twisting, while Mode 5 (2513.2 Hz) displays intricate deformation, indicating a more complex response at higher frequencies.

Table.1.0 Modal analysis of materials at different Modes.

Material	Mode 1 (Hz)	Mode 2 (Hz)	Mode 3 (Hz)	Mode 4 (Hz)	Mode 5 (Hz)
Aluminum Alloy 6061-T6	221.94	224.24	1238.7	1243.1	2782.5
AISI 4140	220.94	223.22	1232.6	1237	2767.4
Ductile Cast Iron	214	216.2	1193.7	1197.9	2679.3
Ti-6Al-4V	102.19	202.28	1118	1122	2513.2

III. RESULTS

The static structural analysis conducted for the drive axle using the four candidate materials under the same loading conditions. The purpose is to assess stress distribution and total deformation, and identify potential failure zones.

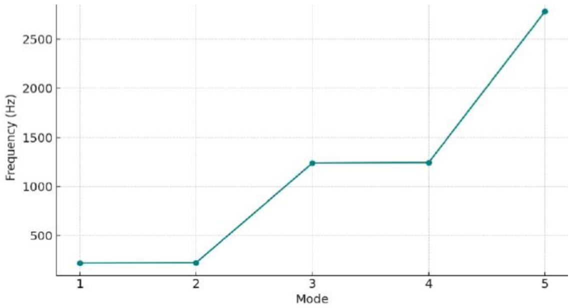

Fig.3.0 Natural Frequencies of Aluminium Alloy 6061-T6

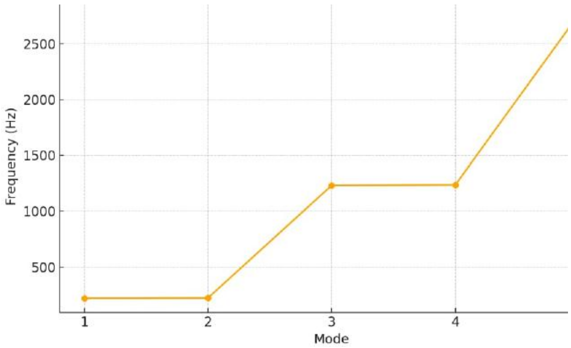

Fig.3.1 Natural Frequencies of– AISI 4140

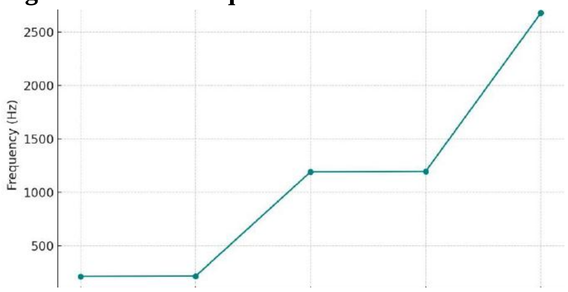

Fig.3.2 Natural Frequencies of Ductile Cast Iron

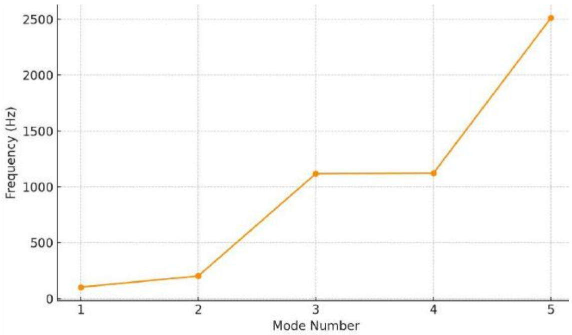

Fig.3.3 Natural Frequencies of Ti-6Al-4V

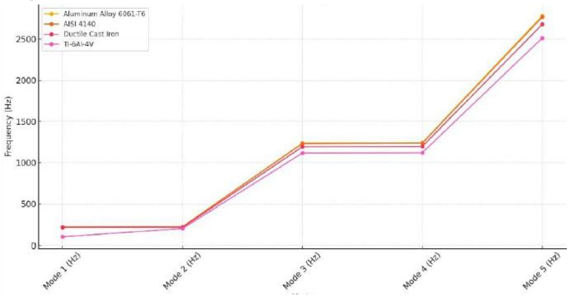

Fig.3.4 Natural Frequencies of various materials.

Aluminium Alloy 6061-T6 consistently shows the highest frequencies across all modes, indicating it is the most resistant to vibration and has the highest stiffness-to-mass ratio.

Ti-6Al-4V consistently has the lowest frequencies, which implies it is more flexible and more susceptible to vibration, though it might still offer good damping properties.

AISI 4140 and Ductile Cast Iron fall in between but follow a very similar trend, showing moderate stiffness and balanced dynamic behavior.

Table.2.0 Maximum and Minimum stress values of various materials.

Material	Max Stress (Pa)	Min Stress (Pa)
Aluminium 6061-T6	7.9318e9	8.307e6
AISI 4140	7.9332e9	9.1814e6
Ductile Cast Iron	7.9336e9	9.1344e6
Ti-6Al-4V (Titanium)	7.944e9	7.2198e6

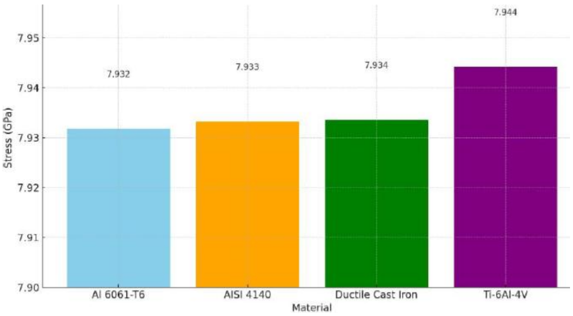

Fig.3.5 Maximum Equivalent Stress comparison

All materials exhibit similar maximum stress levels, indicating they can handle the same applied load under similar design conditions.
Titanium Alloy (Ti-6Al-4V) shows the highest maximum stress, which might indicate better strength properties but could also mean higher stress concentration.
Aluminium 6061-T6 has the lowest maximum stress, suggesting it might distribute the load slightly better, potentially due to lower stiffness.
The differences are minimal (within 0.012 GPa), suggesting geometry has a more dominant effect than material choice in this analysis.

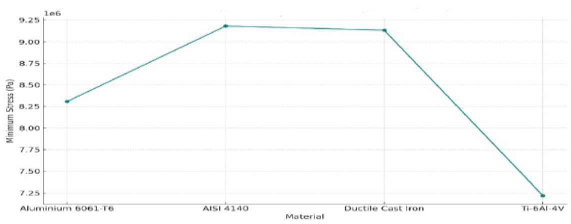

Fig.6.27 Minimum Stress Comparison

AISI 4140 and Ductile Cast Iron show the highest minimum stress values, indicating more uniform stress distribution and possibly better stiffness.
Titanium Alloy (Ti-6Al-4V) shows the lowest minimum stress, suggesting it may have more stress concentration zones or less stiffness under this particular loading.
Aluminium 6061-T6 lies in the mid-range but still closer to titanium than the steels, reflecting its lightweight and flexible nature.

IV. CONCLUSION

This study successfully conducted structural and modal analysis of a heavy-duty drive axle using Finite Element Analysis (FEA) in ANSYS, evaluating four materials: AISI 4140 Steel, Aluminum 6061-T6, Ductile Cast Iron, and Ti-6Al-4V Titanium Alloy. Key findings revealed:
Stress Analysis:
Maximum stresses (~7.93 GPa) consistently occurred at the flange's diameter transition across all materials.
Demonstrated that geometric design influences stress concentration more significantly than material properties.
Deformation Characteristics:
Aluminum 6061-T6 exhibited the highest deformation (36.56 mm)
AISI 4140 Steel showed the least deformation (12.67 mm), making it most suitable for high-stiffness requirements
Vibration Performance:
Modal analysis revealed Aluminum's superior vibration resistance.
Titanium alloy displayed the lowest natural frequencies, potentially increasing resonance risk in dynamic applications.
Material Selection Recommendations:
AISI 4140 Steel: Optimal for conventional heavy-load applications, offering the best balance of strength and stiffness.
Aluminum 6061-T6: Recommended for weight-sensitive applications like electric vehicles, despite higher deformation.
Ti-6Al-4V: Suitable for specialized applications (aerospace/performance EVs) where strength-to-weight ratio justifies cost.
Methodological Contribution:
The study established a replicable framework combining:

- Advanced FEA simulation techniques
- Comprehensive material evaluation
- Multi-criteria decision analysis

This approach provides valuable insights for future drive train component optimization, particularly in the evolving landscape of electric and hybrid heavy vehicles. Future work could explore composite materials and topological optimization to further enhance performance characteristics.

Acknowledgements

An acknowledgement section may be presented after the conclusion, if desired.

REFERENCES

[1]. Kim, T. H., & Jung, Y. H. (2013). Structural analysis of drive axle for durability improvement in commercial vehicles. Journal of Mechanical Science and Technology, 27(5), 1393–1399.

[2]. Khan, S. A., & Gawande, R. S. (2014). Modal and structural analysis of rear axle housing using FEA. International Journal of Engineering Research & Technology (IJERT), 3(7), 123–127.
[3]. Shirbhate, A. M., & Mohite, A. M. (2013). Finite Element Analysis of Rear Axle for Weight Reduction. International Journal of Emerging Technology and Advanced Engineering, 3(5), 588–592.
[4]. Deshmukh, P. S., & Thakare, V. P. (2014). Design and Analysis of Drive Axle for Light Commercial Vehicles. International Journal for Scientific Research & Development (IJSRD), 2(3), 980–984. 67
[5]. Charde, M. S. (2017). Modal Analysis of Axle Using FEA. International Journal of Engineering Sciences & Research Technology (IJESRT), 6(4), 187–191.
[6]. Goyal, R., & Saini, V. (2021). Optimization of axle shaft by weight reduction using finite element analysis. Materials Today: Proceedings, 47, 550–556.
[7]. Sutar, P. P., & Kulkarni, M. M. (2018). Design and analysis of drive axle shaft for medium duty trucks. International Research Journal of Engineering and Technology (IRJET), 5(6), 456–460.
[8]. Patel, R., & Kumar, A. (2019). Finite element-based fatigue analysis of axle shaft. International Journal of Vehicle Structures & Systems (IJVSS), 11(2), 82–86.
[9]. Singh, M., & Verma, N. (2020). Static and dynamic analysis of differential axle housing using ANSYS. International Journal of Engineering and Advanced Technology (IJEAT), 9(3), 178–182.

Books:

[10]. Budynas, R. G., & Nisbett, J. K. (2020). Shigley's Mechanical Engineering Design (11th ed.). McGraw-Hill Education.
[11]. Callister, W. D., & Rethwisch, D. G. (2018). Materials Science and Engineering: An Introduction (10th ed.). Wiley.
[12]. Khurmi, R. S., & Gupta, J. K. (2017). A Textbook of Machine Design. Eurasia Publishing House.
[13]. Rao, S. S. (2017). Mechanical Vibrations (6th ed.). Pearson Education.
[14]. Chandrupatla, T. R., & Belegundu, A. D. (2011). Introduction to Finite Elements in Engineering (4th ed.). Pearson.
[15]. Norton, R. L. (2020). Design of Machinery (6th ed.). McGraw-Hill.
[16]. Juvinall, R. C., & Marshek, K. M. (2020). Fundamentals of Machine Component Design (6th ed.). Wiley.